Molecular Therapy
Nucleic Acids
Original Article

Albumin-conjugation enables improved tumor targeting of aptamers via SPECT imaging

Shaowen Yang,[1,3,4,5] Chengwen Zheng,[1,3,4,5] Sixuan Cheng,[1,3,4] Li Wen,[1,3,4] Pinghui Li,[2] Jianbo Li,[2] Xiaoli Lan,[1,3,4] and Dawei Jiang[1,3,4]

[1]Department of Nuclear Medicine, Union Hospital, Tongji Medical College, Huazhong University of Science and Technology, Wuhan 430022, China; [2]Inner Mongolia Medical University, Hohhot 010050, China; [3]Hubei Province Key Laboratory of Molecular Imaging, Wuhan 430022, China; [4]Key Laboratory of Biological Targeted Therapy, Ministry of Education, Wuhan 430022, China

Aptamers are single-stranded oligonucleotides with specific spatial structures. They have been widely used in preclinical studies because of their high affinity and specificity for various biological targets. AS1411, an aptamer targeting the nucleolin overexpressed on the cancer cell membrane, is one of the most promising and extensively studied aptamers. However, extremely low bioavailability due to rapid renal excretion remains a great obstacle for aptamers' clinical translation. Human serum albumin (HSA), with long blood circulation and excellent biocompatibility, has been an attractive vehicle for extending drugs' blood half-life in the clinic. This work investigated the effect of an albumin-conjugated strategy in improving aptamers' tumor targeting *in vivo* for the first time by taking AS1411 as an example. HSA-AS1411 was synthesized via the maleimide-sulfhydryl reaction. The excellent serum stability and maintained target affinity of HSA-AS1411 were demonstrated *in vitro*. The pharmacokinetic analysis and tumor SPECT imaging studies revealed that HSA-AS1411 had over 14 times longer circulation half-life and superior tumor uptake than those of AS1411. The immunofluorescence staining of tumor tissues further indicated the improved tumor retention of AS1411 as a result of prolonged blood circulation. Therefore, the HSA-conjugated strategy has a promising prospect in improving aptamers' tumor targeting for clinical applications.

INTRODUCTION

Aptamers, single-stranded DNA or RNA molecules, possess unique three-dimensional structures that enable them to bind specifically to a wide array of ions and molecules.[1–5] They exhibit superior affinity and selectivity for these biological targets, presenting several advantages over traditional antibodies, such as cost-effective production, chemical modifiability, enhanced stability, and improved biocompatibility.[6,7] Aptamers function as highly programmable chemical antibodies, and their application in biosensing, bioimaging, and biomedicine has been extensively explored both *in vitro* and *in vivo*, particularly for the precise detection and treatment of cancer.[8–10] For example, Tan and colleagues[11] evaluated the binding specificity of the aptamer SGC8, which targets protein tyrosine kinase 7, in xenograft tumor models and subsequently conducted a phase 0 clinical trial to assess the biosafety and pharmacokinetics of SGC8 in human subjects. Additionally, the aptamer drug pegaptanib, approved by the U.S. Food and Drug Administration in 2004, acts as an antagonist of vascular endothelial growth factor and has shown efficacy in treating exudative age-related macular degeneration.[12]

AS1411, a 26-base guanine-rich aptamer with a distinctive G-quadruplex structure, is among the most promising and extensively studied aptamers.[13] It targets nucleolin, a protein that is overexpressed on the membranes of cancer cells, and has demonstrated significant antitumor activity by upregulating the tumor suppressor gene p53 and downregulating oncogenes Bcl-2 and Akt1.[14] AS1411 has been applied for treating acute myeloid leukemia and renal cell carcinoma in phase II clinical trials,[13,15] marking it as a pioneering anticancer aptamer in human use. However, the clinical usefulness of aptamers is challenged by their susceptibility to nuclease degradation and rapid renal clearance,[16] which limits their theranostic time window and effectiveness. Strategies to enhance their bioavailability, such as chemical modifications in forms of 2′-functionalization, phosphorothioate backbone substitutions, or locked nucleic acids, have been developed to improve aptamers' resistance to nuclease degradation.[17–19] Nevertheless, there is an urgent need for approaches to extend their short circulation half-life (currently 5–10 min)[20] and improve their tumor retention.

Several strategies have been proposed to extend the biological half-life of aptamers. Polyethylene glycol (PEG) modification is a well-established method for prolonging aptamers' blood half-life by increasing

Received 11 September 2024; accepted 6 February 2025;
https://doi.org/10.1016/j.omtn.2025.102483.

[5]These authors contributed equally

Correspondence: Dawei Jiang, PhD, Department of Nuclear Medicine, Wuhan Union Hospital, 1277 Jiefang Avenue, Wuhan 430022, China.
E-mail: daweijiang@hust.edu.cn

their molecular weight beyond the renal filtration threshold.[21–24] However, PEG's immunogenicity can pose challenges in clinical settings, as seen in the severe allergic reactions reported during a phase 2b clinical study of the PEGylated anticoagulant therapy pegnivacogin.[25] Alternatively, small hydrophobic molecules like Evans blue, which have a strong affinity for albumin's hydrophobic pockets, have been explored for modifying aptamers.[26–28] These modifications aim to leverage the hitchhiking effect by binding to endogenous albumins, potentially extending blood circulation. However, the unsatisfying blood half-life and insignificant improvement in tumor uptake have not yet met clinical needs. The complex internal environment can reduce aptamers' affinity to endogenous albumins, and the uncertain binding sites on albumins may weaken aptamers' targeting ability. Thus, there is an urgent need for a more biocompatible, controllable, and effective strategy to promote aptamers for clinical application.

Human serum albumin (HSA), known for its long circulation time and excellent biocompatibility, has been utilized to encapsulate drugs for clinical use, such as in Abraxane.[29] HSA offers a single free sulfhydryl group at the 34th cysteine (cys34) for site-specific covalent binding,[30–32] making it an attractive candidate for the synthesis of a homogeneous and controllable HSA-aptamer complex. This approach can circumvent issues associated with the HSA hitchhike strategy. Kuhlmann et al. have successfully synthesized an HSA-oligonucleotide assembly for potential half-life extension,[33] and confirm the retained bioactivity of aptamers post-conjugation. However, subsequent studies on human FcRn affinity revealed that the HSA-aptamer construct has a 9-fold lower affinity than unmodified HSA unless substituted with a recombinant high-binding albumin variant (HB). This finding is inconsistent with the expected long blood circulation of HSA-aptamer and may hinder the application of HSA-aptamer coupling technology due to uncertain biological safety and challenges in obtaining HB. Nevertheless, numerous studies indicate that *in vitro* analyses may not accurately reflect drugs' pharmacological activity or pharmacokinetic properties in organisms, as they do not closely mimic biological systems.[34–39] Therefore, systematic studies *in vivo* are vital for assessing how the HSA conjugation strategy affects aptamers' bioactivity and blood circulation compared with *in vitro* experiments.

With advancements in molecular imaging technologies such as positron emission tomography (PET) and single photon emission computed tomography (SPECT), the pharmacokinetics and therapeutic efficacy of targeted drugs can be non-invasively visualized and precisely quantified *in vivo*.[40–42] In this study, we synthesized an HSA-aptamer conjugation according to the method reported by Kuhlmann and colleagues[33] with AS1411 as a model and systematically evaluated the impact of the HSA-conjugation strategy on the pharmacokinetics and tumor targeting of AS1411 *in vivo* using SPECT imaging and other nuclear medicine techniques. Our findings strongly support the potential of HSA-AS1411 as an efficient and practical method for improving aptamer blood circulation and tumor retention.

RESULTS

Synthesis of HSA-oligonucleotides

A random sequence (RS) with the same strand length as AS1411 was selected as the control. HSA-AS1411 and HSA-RS were synthesized by a one-step maleimide-sulfhydryl reaction and purified by an ion exchange column (IEX). The specific site-directed synthesis processes were comprehensively delineated in Figure 1. The chromatogram at 260 nm (Figure 2A) showed that HSA was eluted, first because of the lowest negative charge. HSA-AS1411 or HSA-RS had increased negative charges due to conjugated oligonucleotides, thus separated entirely from HSA. The unreacted oligonucleotides were the last to be eluted.

The synthesis and purity of HSA-AS1411 and HSA-RS were investigated by gel electrophoresis. The protein staining (Figure 2B) and DNA staining (Figure 2C) showed the conjugation between HSA and oligonucleotides. HSA-AS1411 and HSA-RS were successfully purified without unreacted HSA or DNA in the product lanes. In addition, since HSA has the only reactive thiol group, HSA-AS1411 and HSA-RS were homogeneous, with only one DNA chain attached. The results of matrix-assisted laser desorption/ionization time-of-flight (MALDI-TOF) (Figure S1) further confirmed the conclusion above.

Excellent serum stability and maintained nucleolin-binding ability of HSA-AS1411 *in vitro*

The serum stability of HSA-AS1411 *in vitro* is vital for AS1411's long-time retained bioactivity after prolonged blood circulation, which was evaluated by agarose gel electrophoresis (Figure 3A) and quantified by the corresponding band intensity (Figure 3B). Overall, HSA-AS1411 and AS1411 exhibited superior serum stability, with more than 50% remaining at 48 h, whereas approximately 90% of HSA-RS and RS were rapidly degraded by the nuclease. This may result from that AS1411 can form a stable G-quadruplex structure resistant to nuclease degradation.[43] Interestingly, approximately 50% of HSA-AS1411 retained the intact structure after 48 h, while AS1411 began to degrade rapidly. The corresponding band intensity of HSA-AS1411 was significantly stronger than AS1411 ($p < 0.001$) at 60 h (Figure 3B). Meanwhile, HSA-RS was also more stable than RS before 36 h ($p = 0.0011$ at 6 h, $p = 0.0018$ at 12 h, and $p = 0.0053$ at 24 h). The results indicated the excellent serum stability of HSA-AS1411. Moreover, the serum stability of AS1411 and RS was improved after coupling with HSA, but whether this effect can be applied to other oligonucleotides remains to be further investigated.

Next, we assessed HSA-AS1411's binding affinity to nucleolins on the cellular level. We selected 4T1 breast cancer cells with high-level expression of the nucleolin[44] and performed the immunofluorescence staining. Both HSA-AS1411 and AS1411 exhibited fast and tight binding to 4T1 cells after being incubated at 37°C for 1 h (Figure 4). This suggested the maintained binding affinity of AS1411 after conjugation to HSA. Meanwhile, we found that the fluorescence signal of AS1411 was located in the nucleus and cytoplasm of 4T1 cells,

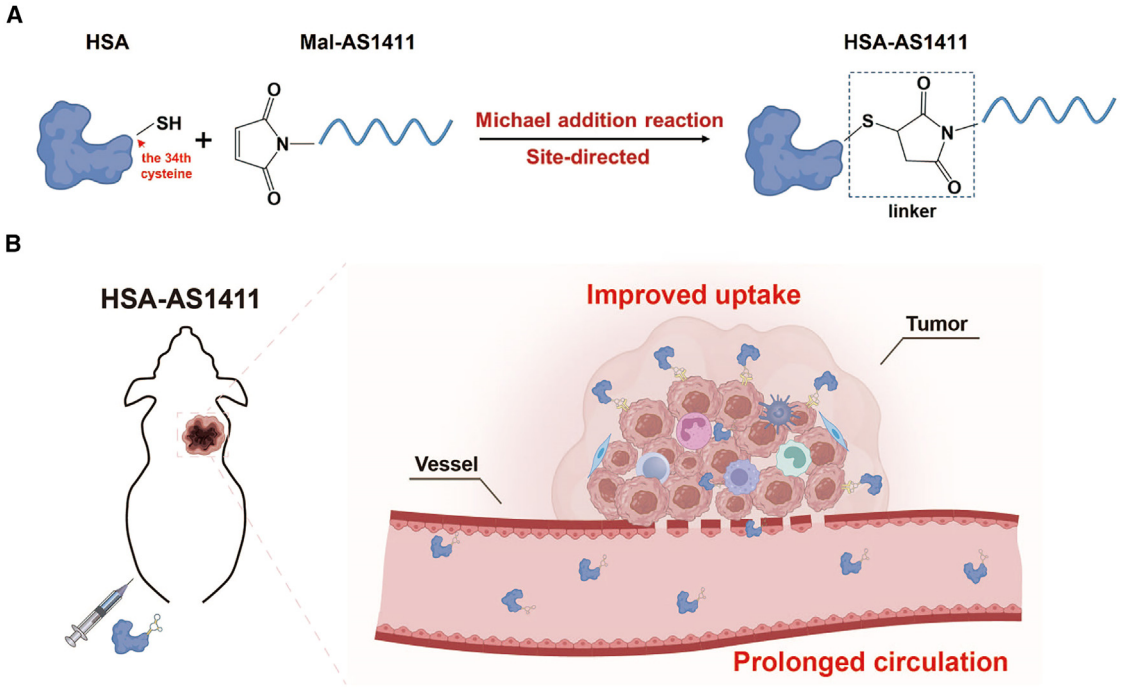

Figure 1. Specific site-directed synthesis processes and excellent in *vivo* effect of HSA-AS1411

(A) The synthesis of HSA-AS1411 involved a Michael addition reaction targeting the only free thiol group on HSA. (B) HSA-AS1411 prolonged the blood circulation and tumor uptake of AS1411 *in vivo*.

whereas HSA-AS1411 was mainly located in the cytoplasm. We will investigate the change of AS1411's location in the subcellular level after HSA conjugation and its impact on the anti-tumor cell proliferation activity of AS1411 in future studies. In summary, HSA-AS1411 demonstrated excellent serum stability and maintained nucleolin affinity *in vitro*, which provided the basis for subsequent *in vivo* studies.

^{99m}Tc radiolabeling of HSA-AS1411

Molecular imaging techniques allow convenient and accurate evaluation of drugs' pharmacokinetics and tumor-targeting in preclinical and clinical studies.[45,46] Technetium-99m (^{99m}Tc, half-life = 6.02 h) was determined as the tracer nuclide for the mild radiolabeling environment and appropriate half-life matched with the expected long blood circulation of HSA-AS1411. We prepared four ^{99m}Tc-labeled probes with high labeling efficiency: ^{99m}Tc-HYNIC-HSA-AS1411, ^{99m}Tc-HYNIC-HSA-RS, ^{99m}Tc-HYNIC-AS1411, and ^{99m}Tc-HYNIC-RS. Their UV chromatograms remained consistent before and after labeling, indicating their chemical stability under the radiolabeling procedure (Figure S2). The radiochemical purity of four ^{99m}Tc-labeled probes was all more than 95% (Figure S3), and their apparent molar activity was 23.18 ± 0.75 MBq/nmol, 23.65 ± 1.59 MBq/nmol, 24.23 ± 2.03 MBq/nmol, and 24.36 ± 1.92 MBq/nmol, respectively. In addition, all four ^{99m}Tc-labeled probes showed good serum stability, retaining above 60% after 36 h (Figures S4–S7). These data allow us to evaluate the pharmacokinetics and tumor uptake of HSA-AS1411 more accurately *in vivo* by nuclear medicine techniques.

Prolonged blood circulation and improved bioavailability of HSA-AS1411

First, we investigated the effect of the HSA-conjugated strategy on prolonging the blood circulation of AS1411 *in vivo*. ^{99m}Tc-HYNIC-HSA-AS1411 was applied for more convenient quantification of HSA-AS1411's plasma concentration, with ^{99m}Tc-HYNIC-AS1411 as the control. A two-compartment model (Figure 5C) was used in the pharmacokinetics study. The radioactive plasma concentration-versus-time curves of the two probes were shown in Figures 5A and 5B, and multiple pharmacokinetics parameters were presented in Figure 5D. The elimination half-life ($T_{1/2\beta}$) of ^{99m}Tc-HYNIC-HSA-AS1411 was 14.28 ± 1.15 h, approximately 14 times that of ^{99m}Tc-HYNIC-AS1411 (0.92 ± 0.49 h). This suggested that the blood half-life of AS1411 is significantly extended after HSA conjugation. The clearance rate (CL) data showed AS1411's rapid clearance from blood, while HSA-AS1411 was retained in the blood for a long time. We also compared the area under the curve (AUC) of them. The $AUC_{0-\infty}$ of ^{99m}Tc-HYNIC-HSA-AS1411 was 101.49 ± 10.07 MBq/L *h, while ^{99m}Tc-HYNIC-AS1411 was only 1.05 ± 0.29 MBq/L *h. This reflected that the bioavailability of AS1411 was greatly increased to 100-fold after HSA conjugation. Overall, the HSA-conjugated strategy has significantly improved the blood

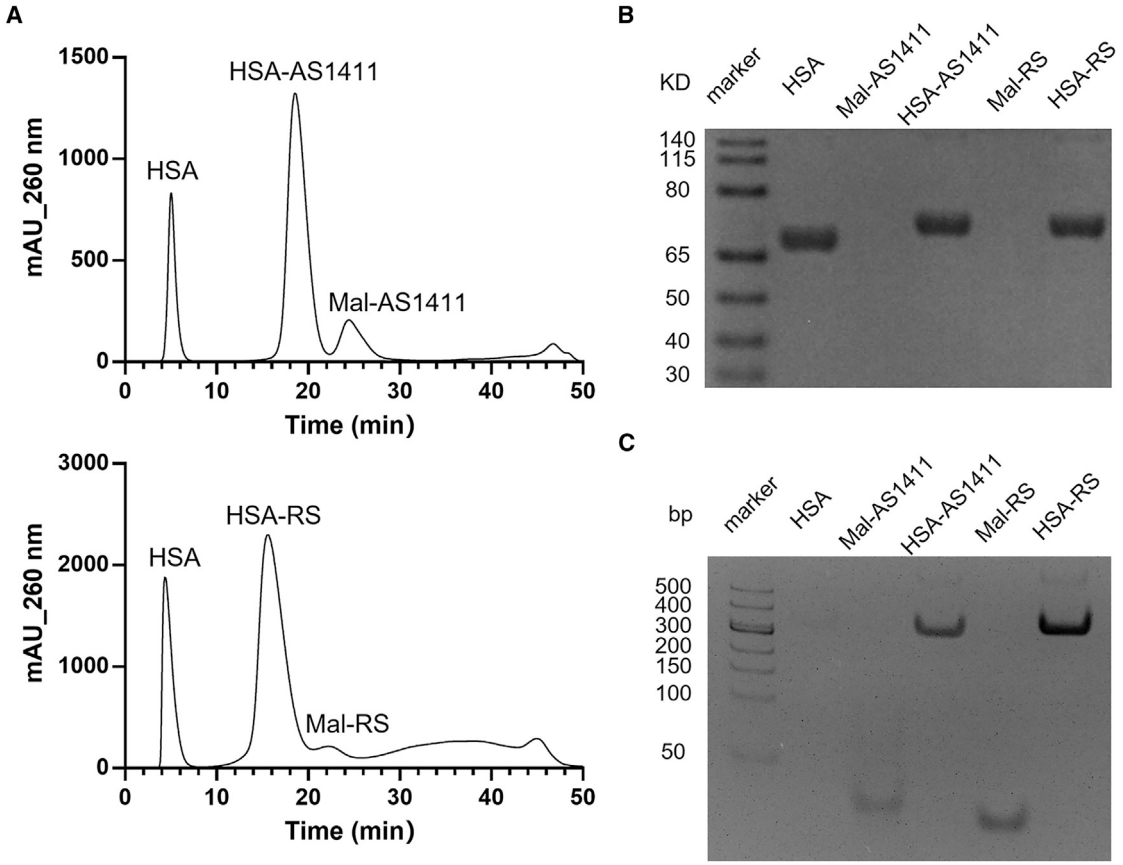

Figure 2. Synthesis and characterization of HSA-AS1411

(A) Purification of HSA-AS1411 and HSA-RS by IEX. The chromatogram at 260 nm showed complete separation of HSA-AS1411 (or HSA-RS) from the mixture. (B) SDS gel electrophoresis. (C) TBE-Urea gel electrophoresis. Coomassie staining (B) and nucleic acid staining (C) co-confirmed the conjugation and purity of HSA-AS1411 (or HSA-RS). Mal, maleimide.

circulation and bioavailability of AS1411, and it is promising to greatly increase AS1411's tumor retention *in vivo*.

HSA-conjugation improves AS1411's tumor-targeting

Next, we evaluated HSA-AS1411's tumor-targeting in 4T1 subcutaneous tumor models by SPECT-computed tomography (SPECT-CT) imaging. As shown in Figures 6A and 6B, ^{99m}Tc-HYNIC-HSA-AS1411 and ^{99m}Tc-HYNIC-HSA-RS exhibited excellent blood circulation, with above 10 percent of injected dose per gram (%ID/g) in the blood at 12 h and around 5%ID/g until 36 h. Their blood pool signals gradually decreased and were finally metabolized by the liver. In contrast, ^{99m}Tc-HYNIC-AS1411 and ^{99m}Tc-HYNIC-RS were rapidly excreted from the body, with a small amount accumulated in the liver, probably due to the lipid solubility brought by the HYNIC. The tumor accumulations of ^{99m}Tc-HYNIC-HSA-AS1411 and ^{99m}Tc-HYNIC-HSA-RS were maintained at a high level and progressively increased as the blood signal declined, with 13.61 ± 1.92%ID/g and 8.60 ± 1.33%ID/g at 36 h, respectively. However, there was almost no radioactivity uptake in the tumors in the group of ^{99m}Tc-HYNIC-AS1411 (0.80 ± 0.07%ID/g at 36 h) and ^{99m}Tc-HYNIC-RS (0.53 ± 0.04%ID/g at 36 h). More notably, the tumor uptake of ^{99m}Tc-HYNIC-HSA-AS1411 was significantly higher than ^{99m}Tc-HYNIC-HSA-RS after 12 h as the blood concentration decreased (p = 0.0209 at 12 h and p = 0.0252 at 36 h) (Figure 6B), suggesting that, in addition to the enhanced permeability and retention (EPR) effect, the increased tumor uptake was partly attributed to the improved tumor-targeting of AS1411.

The *ex vivo* distribution study at 36 h post-injection (Figures 6C and S9; Table S1) also confirmed the tumor uptake of ^{99m}Tc-HYNIC-HSA-AS1411 was significantly higher than other groups. Among them, the HSA-AS1411 group was approximately 26 times higher than AS1411. Meanwhile, its blood radioactive signal intensity was about 33 times the AS1411 group. These data more directly demonstrated the excellent effect of HSA conjugation in prolonging blood circulation and improving tumor accumulation of AS1411. We also calculated the radioactivity radio of tumor to blood (T/B) and tumor to muscle (T/M) in the HSA-AS1411 and HSA-RS groups to

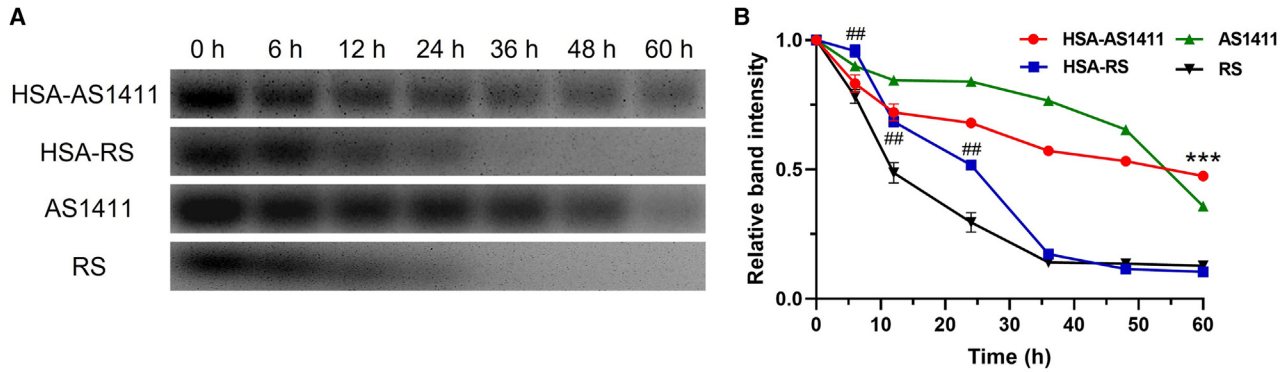

Figure 3. Evaluation of HSA-AS1411's serum stability

HSA-AS1411, HSA-RS, and corresponding bare oligonucleotides were incubated with 50% FBS at RT. The aliquots (n = 3) were collected and resolved by agarose gel electrophoresis (A). The bands were quantified by ImageJ and the relative band intensity-time curve was plotted (B). ***Significant difference between HSA-AS1411 and AS1411 group ($p < 0.001$), ##Significant difference between HSA-RS and RS group ($p < 0.01$). Error bars show SD.

eliminate the EPR effects in tumor uptake. The ratio of T/M showed a significant difference ($p = 0.0229$), while the difference of T/B was not ($p = 0.1242$) (Figure 6D).

To further validate that the HAS-conjugated strategy improves the tumor-targeting of AS1411, we performed immunofluorescence staining of the tumor sections to visualize the specific binding of AS1411 to the nucleolin expressed in tumors (Figure 7). The cyanine 3 (Cy3)-modified HSA-AS1411 exhibited high fluorescence intensity in tumor tissues, with a part co-localized with the nucleolin. In contrast, Cy3-HSA-RS had only a moderate fluorescence signal, and Cy3-AS1411 or Cy3-RS had almost no signal in tumor sections. This further illustrates that the HSA conjugation increased the tumor uptake of AS1411, leading to a prolonged interaction with the nucleolin overexpressed on tumor cells, thus improving the tumor-targeting ability of AS1411.

HSA-AS1411 is biocompatible for potential clinical applications

Finally, we assessed the biocompatibility of HSA-AS1411 for potential clinical studies in the future. After 36 h intravenous injection, the hematoxylin and eosin (H&E) staining of HSA-AS1411's major retention and metabolizing organs (including the heart, liver, and kidney) showed no obvious organ toxicity (Figure S8). This suggests that HSA-AS1411 has a good prospect of clinical application for its promising biosafety.

DISCUSSION

The emergence of tumor-targeting drugs has transformed the traditional paradigm of cancer diagnosis and treatment.[47] Compared with traditional chemotherapeutic drugs, they have efficient anticancer effects with less toxicity to healthy tissues, making tumor-targeted imaging more precise and therapy more effective in clinical settings.[48] As novel tumor-targeting agents, aptamers have received increasing attention in preclinical and clinical studies. Currently, the most urgent issue for aptamers' clinical applications is how to extend their biological half-life and increase their bioavailability, thereby maximizing the therapeutic benefit to patients.

In this study, HSA was determined as the carrier in the novel aptamer blood half-life extending strategy, considering its excellent biocompatibility and extensive drug delivery applications. We synthesized a homogeneous HSA-AS1411 complex with only one aptamer attached to the only free sulfhydryl group on HSA (Figures 2 and S1). Moreover, the coupling site is located in the domain I of HSA, which is distant from the primary neonatal Fc receptor (FcRn) engagement site in domain III.[49] This offers the opportunity that HSA-AS1411 will maintain the affinity to FcRn and have a long blood circulation like HSA.

There are two prerequisites for the effectiveness of blood circulation-extending strategies for aptamers *in vivo*: good serum stability and sustained tumor-targeting ability. First, aptamers' serum stability must be matched to the extended long blood circulation, which implies a prolonged interaction with serum nuclease. However, due to the susceptibility to nuclease, most unmodified aptamers can only maintain structurally stable in the serum for minutes to a few hours.[50] This leads to the fact that most aptamers are rapidly degraded and lose bioactivity after being injected intravenously, with only a small amount reaching the tumor site. Thus, we confirmed the excellent serum stability of HSA-AS1411 *in vitro* before *in vivo* studies. Benefiting from AS1411's inherent anti-nuclease degradation ability, HSA-AS1411 can accumulate a high concentration with retained nucleolin-targeting ability at the tumor site for a long time, resulting in high uptake by tumors. However, serum stability improvement technologies are recommended for other aptamers. Second, blood circulation-extending strategies are usually achieved by modifying small hydrophobic chemical agents that can be inserted into endogenous albumin,[26–28,51] or coupling them with long-circulating biomolecules such as albumin, IgG FcRn, and the albumin-binding domain (ABD).[52–56] The evaluation of aptamers' targeting affinity is crucial after modification or conjugation strategies, because the formation of aptamers' specific structure may be affected due to the steric

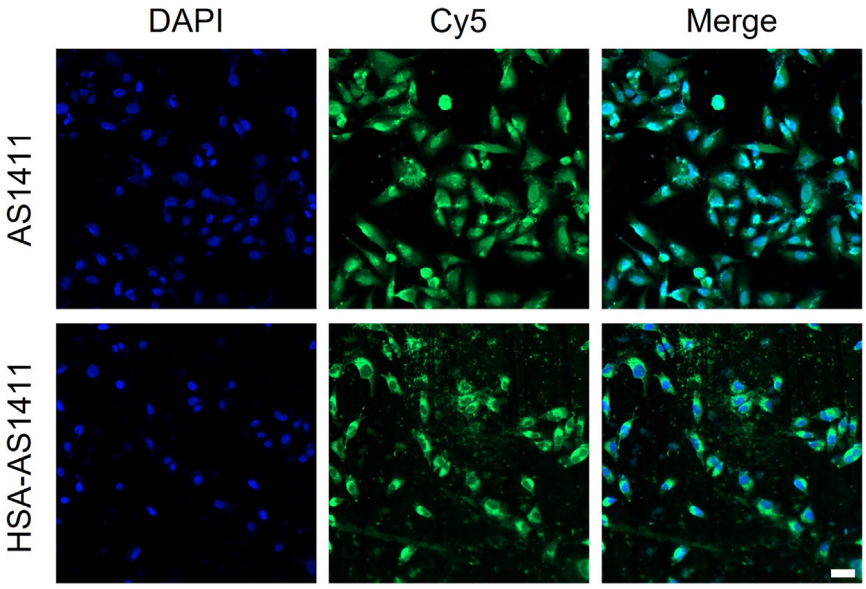

Figure 4. Immunofluorescence staining to investigate the nucleolin-targeting ability of HSA-AS1411 in 4T1 breast cancer cells
Scale bar, 50 μm. Cy5, cyanine 5.

hindrance effect. These two prerequisites may provide support for the development of blood circulation-extending strategies.

Molecular imaging, or more specifically, nuclear medicine, enables us to evaluate the effect of blood circulation extending strategies on tumor-targeting drugs more conveniently and accurately.[57] With regard to the modification of aptamer drugs, the effect includes two aspects: the prolonged blood half-life and increased tumor uptake. The high radiochemical purity (RCP) and expected serum stability of the prepared ^{99m}Tc-labeled HSA-AS1411 allowed us to accurately and quantitatively evaluate the effect of HSA conjugation on AS1411 *in vivo*. As shown in Figures 5 and 6, HSA-AS1411 has a 14-fold increase in blood half-life and nearly 100-fold improvement in bioavailability (presented as AUC) compared with AS1411. The tumor uptake of the HSA-AS1411 group is 26 times higher than the AS1411 group at 36 h. Moreover, our results suggest the HSA conjugation has not only increased AS1411's tumor uptake through the EPR effect but also improved its tumor retention via aptamer specific binding to its target. We speculated that the high tumor accumulation of HSA-AS1411 increased the probability of the interaction with the nucleolin highly expressed on 4T1 cells, thus improving the nucleolin-targeting ability of AS1411.

The significant limitation of the HSA-conjugated strategy is its sustained massive liver uptake, which could hinder subsequent therapeutic studies combining chemotherapy or radioimmunotherapy.[58,59] HSA's high molecular weight (~66 kDa) and ultimate metabolism by the liver may account for this. In addition, HSA-AS1411's excessive blood circulation may lead to the adsorption of large amounts of endogenous albumin, making inevitable high liver uptake.[60] Therefore, the critical challenge for aptamers' blood circulation-extending strategies is to search for chemical or protein molecules with the following properties: (1) appropriate affinity for endogenous albumin, (2) small molecular weights and can rapidly excreted from the kidneys or intestines, and (3) excellent biocompatibility. Based on these, our group has selected some hydrophobic chemical molecules as candidates and achieved some initial satisfactory results. Meanwhile, the ABD is also a promising candidate, a small, three-helical protein domain that has completed extending the blood half-life of peptides and antibody fragments.[54,56] We will evaluate the effect of ABD on aptamers' blood circulation in future research.

In conclusion, the HSA-conjugated strategy has significantly prolonged AS1411's blood circulation and improved its tumor-targeting ability. Considering the excellent biocompatibility of HSA, we hold great promise that this strategy will greatly improve aptamers' tumor-targeting therapeutic effects and promote their clinical applications in the future.

MATERIALS AND METHODS

Materials

HSA was obtained from Biosharp (Beijing, China). 4S Red Plus Nucleic Acid Gel Stain 10,000× was purchased from Sangon Biotech (Shanghai, China). SDS Running Buffer (20×), Tris Acetate-EDTA (TAE) Buffer (10×), and Tris-borate-EDTA (TBE) Buffer (10×) were purchased from ThermoFisher (Shanghai, China). We obtained 2% NA-Red agarose gel, SDS-poly (acrylamide) gel electrophoresis (SDS-PAGE) Gel Preparation Kit, TBE-urea poly (acrylamide) gel electrophoresis (TBE-Urea PAGE) Preparation Kit, and BCA Protein Assay Kit from Beyotime Biotechnology (Shanghai, China). Fast Coomassie Brilliant Blue Staining Solution (10×) and 4′,6-diamidino-2-phenylindole (DAPI) were obtained from Elabscience (Wuhan, China). N-Hydroxysuccinimide ester of hydrazinonicotinic acid (HYNIC-NHS ester) was purchased from Ruixibio (Xi'an, China). All other unbranded chemical agents were purchased from Aladdin Industrial Corporation (Shanghai, China).

All DNA strands with or without modification, were synthesized by Sangon Biotech (Shanghai, China) without further purification. AS1411: 5′-TTTTGGTGGTGGTGGTTGTGGTGGTGGTGG-3′. RS: 5′-TTTTNNNNNNNNNNNNNNNNNNNNNNNN-3′, N refers to random bases.

Synthesis of HSA-oligonucleotides

AS1411 was modified with Mal at the 5′ end by Sangon Biotech. Mal-AS1411 was dissolved in the nuclease-free water before the reaction. The concentration of Mal-AS1411 was measured at A260 on a

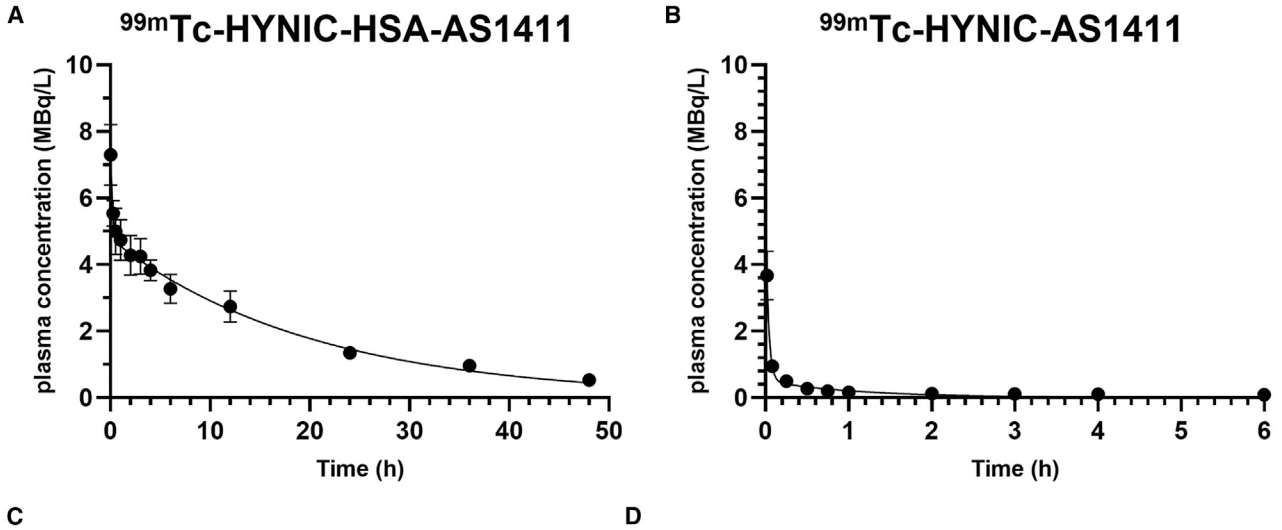

C

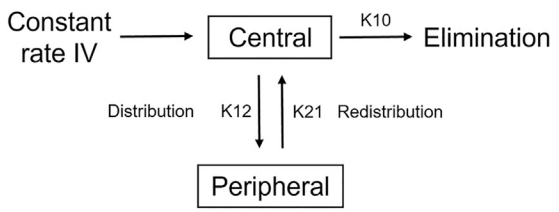

D

Parameter	Unit	^{99m}Tc-HYNIC-HSA-AS1411	^{99m}Tc-HYNIC-AS1411
C_{max}	MBq/L	7.29 ± 0.91	3.67 ± 0.73
T_{max}	h	0.0167	0.0167
AUC $_{0-t}$	MBq/L * h	90.71 ± 9.62	0.84 ± 0.09
AUC $_{0-\infty}$	MBq/L * h	101.49 ± 10.07	1.05 ± 0.29
CL	L/h/MBq	6.72 ± 0.44	811.28 ± 206.92
K10	1/h	0.08 ± 0.03	6.06 ± 2.80
K12	1/h	1.27 ± 0.19	20.26 ± 4.80
K21	1/h	2.35 ± 0.76	3.49 ± 1.12
$T_{1/2\alpha}$	h	0.16 ± 0.09	0.03 ± 0.01
$T_{1/2\beta}$	h	14.28 ± 1.15	0.92 ± 0.49
MRT	h	15.22 ± 0.39	1.77 ± 0.10

Figure 5. Pharmacokinetics study of ^{99m}Tc-HYNIC-HSA-AS1411

The radioactive concentration of plasma (n = 5) was presented in terms of MBq/L. The plasma concentration versus time curves were analyzed by a two-compartmental model. (A and B) The plasma concentration versus time curves of ^{99m}Tc-HYNIC-HSA-AS1411 and ^{99m}Tc-HYNIC-AS1411. Error bars show SD. (C) The illustration of the two-compartmental model. IV, intravenous injection. (D) Pharmacokinetic parameters calculated by DAS 2.0.

microplate reader (Bio-Rad; Hercules, CA, USA). HSA (powder, 5 equivalents [eq.]) was added to the Mal-AS1411 solution and dissolved completely by ultrasound. The reaction was carried out at 400 rpm overnight at room temperature (RT). HSA-RS was synthesized in the same way.

IEX purification

HSA-AS1411 and HSA-RS were purified by an AKTA pure protein purification system (GE Healthcare; Little Chalfont, Buckinghamshire, UK). The system was equipped with IEX (Hitrap Capto ImpRes Q 1*1 mL; GE Healthcare). The mixtures were eluted with A (20 mM Tris-HCl and 10 mM NaCl) and B (20 mM Tris-HCl and 1M NaCl), using a flow rate of 0.4 mL/min at RT. The gradient was 40% B at 0 min, increased from 40% to 80% B in 40 min, then from 80% to 100% B in 5 min, and finally kept at 100% B for 5 min. The collected fractions were desalted and concentrated with nuclease-free water washing three times in Millipore 10 kDa ultrafiltration tubes. The purified products were quantified with the BCA Protein Assay kit and stored lyophilized at −20°C.

MALDI-TOF analysis

MALDI-TOF experiments were performed by a RapifleX MALDI-TOF/TOF. HSA was used as the standard, and 1 μL standard and desalted samples were taken onto the sample target. After drying naturally, 0.6 μL CHCA was brought onto the corresponding target and dried naturally. The molecular weight of the samples was tested after calibrating the sample target with the test standard. The laser source was 335 nm, and the scanning range was 1000–80000 Da. The raw data and plots generated by MALDI-TOF/TOF were analyzed and processed by flexAnalysis (Bruker Daltonics GmbH, Germany).

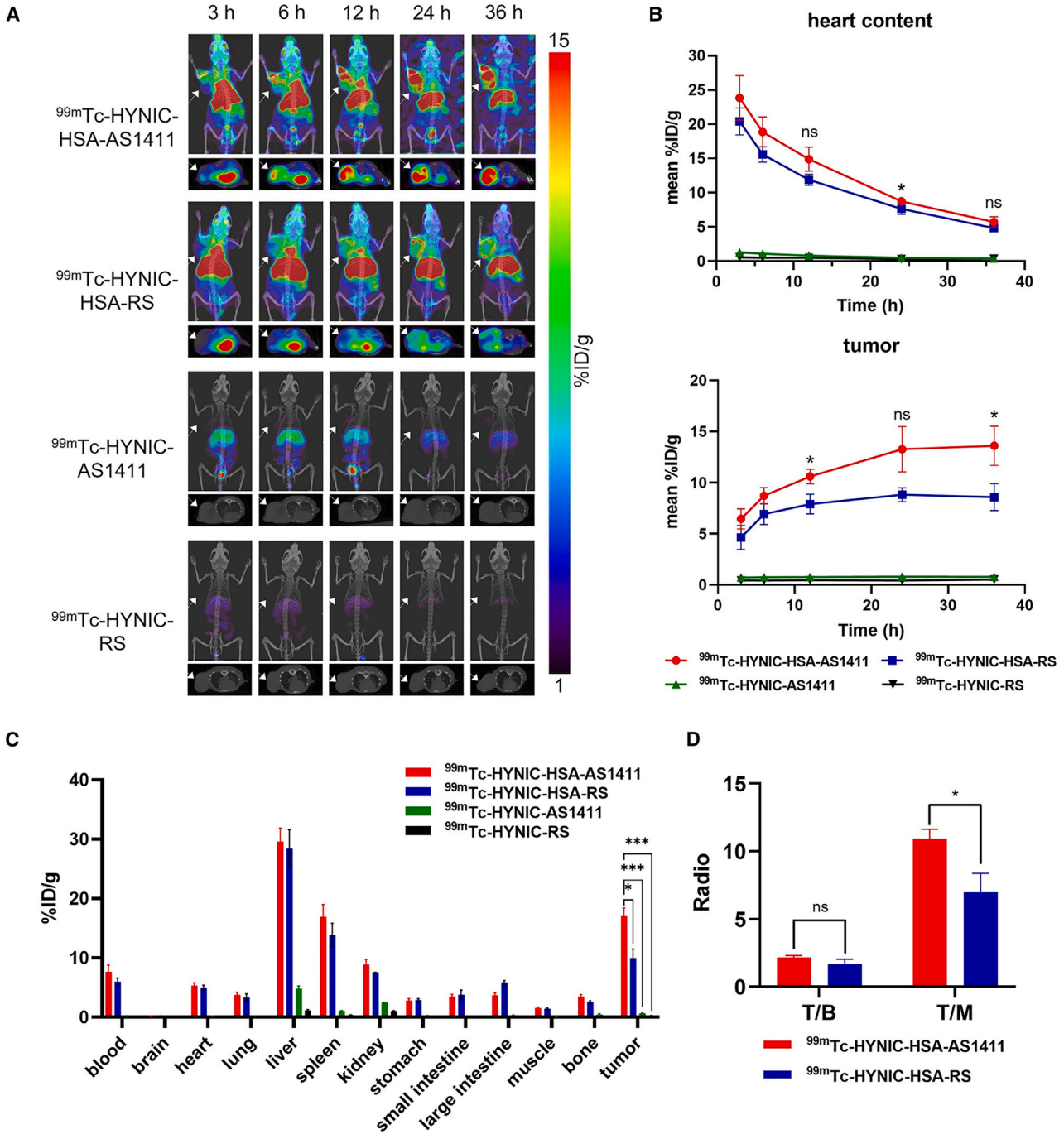

Figure 6. SPECT-CT imaging and 36 h biodistribution study of the four probes (^{99m}Tc-labeled HSA-AS1411, HSA-RS, AS1411, and RS) in 4T1 subcutaneous tumor models (n = 3)

(A) SPECT-CT images for multiple periods (3, 6, 12, 24, and 36 h). The arrow refers to the tumor. (B) Radioactive signal intensity-time curves of heart content and tumor. * and ns represent the significant difference between ^{99m}Tc-HYNIC-HSA-AS1411 and ^{99m}Tc-HYNIC-HSA-RS. (C) Radioactive counts of *ex vivo* organs and tissues by the gamma counter at 36 h after post-injection. (D) Comparison of T/B and T/M between ^{99m}Tc-HYNIC-HSA-AS1411 and ^{99m}Tc-HYNIC-HSA-RS. Error bars show SD. ***$p < 0.001$; *$p < 0.05$; ns, no significance.

Gel electrophoresis

SDS-PAGE and TBE-Urea PAGE were used to assess the conjugation and purity of HSA-AS1411 and HSA-RS with protein staining and DNA staining, respectively. Briefly, 8% SDS-poly (acrylamide) gels and 8% TBE-urea poly (acrylamide) gels were prepared according to instructions provided by Beyotime Biotechnology. SDS-PAGE was run at 120 v for 50 min. TBE-Urea PAGE was run at 150 v for 60 min. SDS gels were stained with Coomassie brilliant blue, and TBE-Urea gels were stained with 4S Red Plus Nucleic Acid Gel Stain after the electrophoresis. Gels were scanned using a gel imaging scanner (Analytik Jena; Jena, Germany). Coomassie was detected by white light, and 4S Red Plus was detected by ultraviolet light.

Serum stability evaluation

We incubated 100 pmol of HSA-AS1411, HSA-RS, AS1411, and RS in 50% FBS (HyClone; Logan, Utah, USA) for 0, 6, 12, 24, 36, 48, and 60 h at RT, respectively. Samples were then collected and analyzed using 2% NA-Red agarose gel electrophoresis with 1× TAE as the running buffer. The gel images were acquired by a gel imaging scanner, and the band intensity was quantified by ImageJ.

Cell lines and cell culture

The 4T1 mouse breast cancer cell line was obtained from the Shanghai Type Culture Collection of the Chinese Academy of Sciences. 4T1 cells were cultured in DMEM medium (Gibco; Grand Island, NY, USA) including 10% FBS (Gibco) and 1% penicillin-streptomycin (Procell, Wuhan) at 37°C and 5% CO_2 atmosphere. The 4T1 cells were used for subsequent experiments when reaching the logarithmic growth phase.

Cellular immunofluorescence staining to investigate HSA-AS1411's binding affinity to the nucleolin

We inoculated 4T1 cells onto 14-mm glass coverslips (Biosharp) at the density of 5×10^4 and incubated overnight. Then, the cells were incubated with 200 pmol/mL Cy5 modified HSA-AS1411 or AS1411 in the serum-free culture medium for 1 h at 37°C and washed three times with PBS. Cells were fixed with 4% paraformaldehyde solution (Solarbio, Beijing, China) for 10 min at RT. After washing three times again with PBS, cells were stained with DAPI for 10 min at RT. Finally, they were incubated in the Antifade Mounting Medium (Beyotime) and imaged by the automatic slice scanning system (OLYMPUS; VS120).

Synthesis of ^{99m}Tc radiolabeled HSA-AS1411

HSA-AS1411 and HSA-RS were dissolved in PBS, while NH_2-AS1411 and NH_2-RS were dissolved in a carbonate buffer (pH = 8.5) for better chelator modification efficiency. HYNIC-NHS ester (dissolved in DMSO, 30 eq.) was added to the solution and reacted overnight at 4°C away from light for the synthesis of HYNIC-HSA-AS1411, HYNIC-HSA-RS, HYNIC-AS1411, and HYNIC-RS. The mixtures were purified with NAP-5 columns (Cytiva, Marlborough, MA, USA) to remove excess HYNIC-NHS ester.

The ^{99m}Tc radiolabeling procedure followed the reported methods. In brief, tricine (0.1 mg) and $SnCl_2$ (30 μg) were added to the HYNIC-HSA-AS1411 solution and mixed with $^{99m}TcO_4^-$ eluate (500 μL, 1,110 MBq; eluted from ^{99m}Tc/^{99}Mo generator). The mixture was shaken at RT for 30 min, then purified with a PD-10 desalting column (GE Health) to obtain ^{99m}Tc-labeled HYNIC-HSA-AS1411. The other three probes were obtained similarly: ^{99m}Tc-HYNIC-HSA-RS, ^{99m}Tc-HYNIC-AS1411, and ^{99m}Tc-HYNIC-RS. Quality control was performed to investigate the stability of four probes under the radiolabeling environment by high-performance liquid chromatography (Shimadzu, Kyoto, Japan). The apparent molar activity of four ^{99m}Tc-labeling probes was calculated and presented as MBq/nmol. The RCP was determined by radio-ITLC (mobile phase: acetone).

The serum stability of ^{99m}Tc-HYNIC-HSA-AS1411, ^{99m}Tc-HYNIC-HSA-RS, ^{99m}Tc-HYNIC-AS1411, and ^{99m}Tc-HYNIC-RS was investigated. After being incubated in 50% FBS at RT for multiple periods (6, 12, 24, and 36 h), the RCP of samples was measured by radio-ITLC, and the radioactive serum stability of four probes was reflected by the RCP at different time points.

Animals and tumor modeling

All animal experiments followed the Institutional Animal Care and Use Committee of Huazhong University of Science and Technology-approved protocol. Female BALB/c mice (4–6 weeks old) were provided by Henan Skobes Biotechnology Co., Ltd. All mice were fed with standard diets and water. We inoculated 100 μL 4T1 cell suspension (containing 1×10^7 cells) into the right axilla of each mouse for subcutaneous xenograft model construction. Mice with 200–400 mm^3 tumor volumes were used *in vivo* tumor-targeting studies.

Pharmacokinetics study

The healthy BALB/c mice were injected with 37 MBq of ^{99m}Tc-HYNIC-HSA-AS1411 via the tail vein. ^{99m}Tc-HYNIC-AS1411 with the same radioactive dose served as the control group. Blood samples were collected from the retro-orbital vein of mice with capillary tubes at multiple time points (^{99m}Tc-HYNIC-HSA-AS1411: 0.0167, 0.25, 0.5, 1, 2, 3, 4, 6, 12, 24, 36, and 48 h; ^{99m}Tc-HYNIC-AS1411: 0.0167, 0.0833, 0.25, 0.5, 0.75, 1, 2, 3, 4, and 6 h). They were weighted, and the radioactivity was measured by a gamma counter (2470, WIZARD; PerkinElmer, Waltham, MA, USA). The plasma concentration was presented in terms of MBq/L and analyzed by a two-compartmental model after attenuation correction. The plasma concentration versus time curves were drawn by the GraphPad Prism software (version 9.5, La Jolla, CA, USA).

Pharmacokinetic parameters were calculated by DAS 2.0 (BioGuider Co., Shanghai, China), including the following: maximum plasma concentration, time to reach maximum plasma concentration; area under the plasma concentration-time curve from zero (predose) to infinity ($AUC_{0-\infty}$); area under the plasma concentration-time curve from zero (predose) to the last time point (AUC_{0-t}); CL; distribution rate constant (K10, K12, and K21); distribution half-life ($T_{1/2\alpha}$); $T_{1/2\beta}$; and mean residence time.

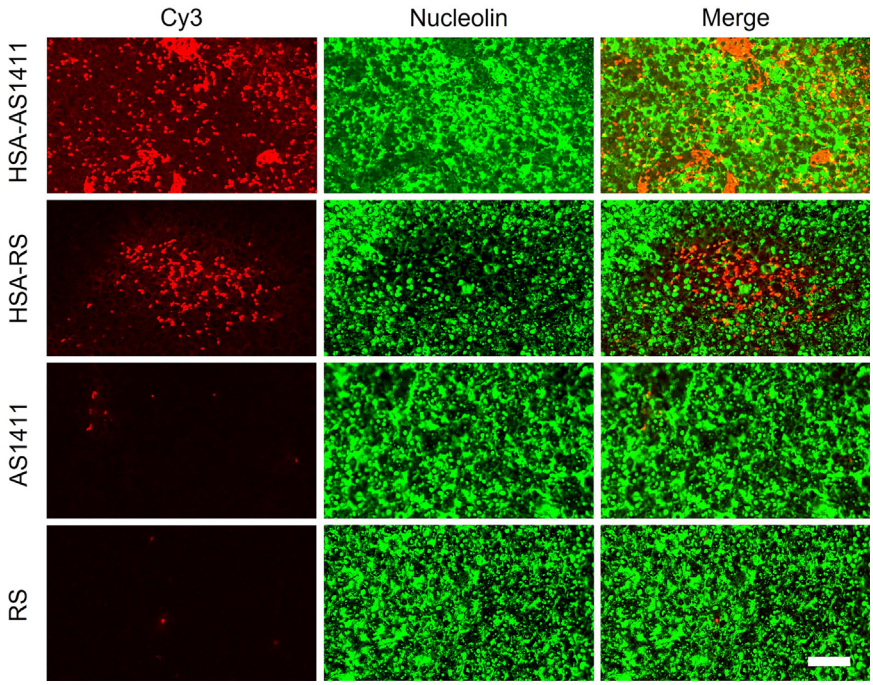

Figure 7. Immunofluorescence staining of 4T1 tumors collected from the four Cy3-modified probes treatment groups (Cy3-HSA-AS1411, Cy3-HSA-RS, Cy3-AS1411, and Cy3-RS)

The yellow color means the co-localization of Cy3-HSA-AS1411 and nucleolin. Scale bar, 50 μm.

SPECT-CT imaging and *ex vivo* biodistribution

Mice with 200–400 mm^3 tumor volumes were randomly divided into four groups for SPECT-CT imaging and *ex vivo* biodistribution. We injected 37 MBq of ^{99m}Tc-HYNIC-HSA-AS1411, ^{99m}Tc-HYNIC-HSA-RS, ^{99m}Tc-HYNIC-AS1411, and ^{99m}Tc-HYNIC-RS via the tail vein, respectively. All images were acquired by the micro-PET/SPECT-CT multimodal imaging system (InliView-3000B, Novel Medical, Yongxin Medical Equipment Co., Ltd., Beijing, China). The mice were anesthetized by isoflurane inhalation during the scanning duration. Statistic scanning was performed at 3, 6, 12, 24, and 36 h after injection. Maximum intensity projection and transaxial images were shown using the NMSoft-ALWS V1.8 software (Novel Medical). For quantitative analysis, regions of interest of heart content (i.e., blood pool) and tumors were delineated on selected transaxial images, and the radioactive counts were presented in terms of %ID/g.

The *ex vivo* biodistribution studies were performed at 36 h after injection to quantify the uptake of four radiolabeling probes in organs/tissues. The mice were sacrificed, and multiple organs/tissues (including the blood, brain, heart, lung, liver, spleen, kidney, stomach, small intestine, large intestine, muscle, bone, and tumor) were collected. The radioactivity of organs/tissues was quantified by the gamma counter. The biodistribution data were represented as %ID/g after attenuation correction. T/B and T/M were calculated to eliminate the effects of radioactive signals in the blood pool.

Immunofluorescence staining of tumor sections

Mice with 200–400 mm^3 tumor volumes were randomly divided into four groups and injected with Cy3-HSA-AS1411, Cy3-HSA-RS, Cy3-AS1411, and Cy3-RS via the tail vein, respectively. The mice were euthanized after 36 h, and tumor tissues were collected, washed three times with PBS, fixed in the 4% paraformaldehyde solution, and embedded in the paraffin. After being cut into 5-mm slices, they were blocked with BSA (Solarbio) and incubated with an anti-nucleolin primary polyclonal antibody (Sanying, Wuhan; 10556-1-ap) overnight at 4°C. Then the tumor tissue slices were treated with fluorescein isothiocyanate-labeled secondary antibody (Thermo Fisher Scientific; Waltham, MA, USA; F2761) away from light for 50 min at RT. After being washed with PBS three times, DAPI was added to stain the nuclei for 10 min at RT. The multi-channel fluorescence images of tumor sections were obtained by the fluorescence microscope and processed by ImageJ.

Biosafety assessment of HSA-AS1411

The healthy BALB/c mice were randomly divided into three groups to assess the biosafety of HSA-AS1411, with AS1411 and saline as the control. In detail, HSA-AS1411, AS1411, and an equal volume of saline were injected via the tail vein, respectively. The mice were euthanized after 36 h. The main retention and metabolizing organs (the heart, liver, and kidney) were dissociated, sliced, and stained by the H&E solution. Images were obtained by the microscope.

Statistical analysis

Statistical analysis and charting were performed by the GraphPad Prism software (version 9.5). All data were shown as mean ± SD. Statistical analysis was performed using the unpaired Student's t test (two-tailed). Differences were considered statistically significant when p values were less than 0.05.

DATA AVAILABILITY

All data generated or analyzed in this study are available upon reasonable request.

ACKNOWLEDGMENTS

This work was supported by the National Key Research and Development Program of China (2022YFB3808200), National Natural Science Foundation of China (22277031, 82102121), and Open Program of Hubei Province Key Laboratory of Molecular Imaging (No. 2023fzyx011).

AUTHOR CONTRIBUTIONS

D.J. conceived and supervised the work. S.Y. and C.Z. conducted the experiments and analyzed the results. S.Y. wrote the manuscript. S.C. provided advice on drawing figures.

L.W. and P.L. provided assistance in the experiments. D.J., J.L., and X.L. revised the manuscript.

DECLARATION OF INTERESTS

The authors declare no competing interests.

SUPPLEMENTAL INFORMATION

Supplemental information can be found online at https://doi.org/10.1016/j.omtn.2025.102483.

REFERENCES

1. Chen, S., Zhang, L., Yuan, Q., and Tan, J. (2022). Current Advances in Aptamer-based Biomolecular Recognition and Biological Process Regulation. Chem. Res. Chin. Univ. *38*, 847–855.
2. Miao, Y., Gao, Q., Mao, M., Zhang, C., Yang, L., Yang, Y., and Han, D. (2021). Bispecific Aptamer Chimeras Enable Targeted Protein Degradation on Cell Membranes. Angew Chem. Int. Ed. Engl. *60*, 11267–11271.
3. Sun, W., Du, L., and Li, M. (2010). Aptamer-based carbohydrate recognition. Curr. Pharm. Des. *16*, 2269–2278.
4. Zhu, H., Wu, E., Pan, Z., Zhang, C., Zhang, Y., Liao, Q., Wang, Y., Sun, Y., Ye, M., and Wu, W. (2023). Development of an Aptamer-Based Molecular Tool for Specifically Targeting Microglia via the CD64 Protein. Anal. Chem. *95*, 3238–3246.
5. Azzouz, A., Hejji, L., Kumar, V., and Kim, K.-H. (2023). Nanomaterials-based aptasensors: An efficient detection tool for heavy-metal and metalloid ions in environmental and biological samples. Environ. Res. *238*, 117170.
6. Fu, Z., and Xiang, J. (2020). Aptamer-Functionalized Nanoparticles in Targeted Delivery and Cancer Therapy. Int. J. Mol. Sci. *21*, 9123.
7. Zhou, J., and Rossi, J. (2017). Aptamers as targeted therapeutics: current potential and challenges. Nat. Rev. Drug Discov. *16*, 181–202.
8. Kou, X., Zhang, X., Shao, X., Jiang, C., and Ning, L. (2020). Recent advances in optical aptasensor technology for amplification strategies in cancer diagnostics. Anal. Bioanal. Chem. *412*, 6691–6705.
9. Meng, H.-M., Liu, H., Kuai, H., Peng, R., Mo, L., and Zhang, X.-B. (2016). Aptamer-integrated DNA nanostructures for biosensing, bioimaging and cancer therapy. Chem. Soc. Rev. *45*, 2583–2602.
10. Wu, H., Lin, J., Ling, N., Zhang, Y., He, Y., Qiu, L., and Tan, W. (2024). Functional Nucleic Acid-Based Immunomodulation for T Cell-Mediated Cancer Therapy. ACS Nano *18*, 119–135.
11. Ding, D., Zhao, H., Wei, D., Yang, Q., Yang, C., Wang, R., Chen, Y., Li, L., An, S., Xia, Q., et al. (2023). The First-in-Human Whole-Body Dynamic Pharmacokinetics Study of Aptamer. Research *6*, 0126.
12. Takeda, A.L., Colquitt, J., Clegg, A.J., and Jones, J. (2007). Pegaptanib and ranibizumab for neovascular age-related macular degeneration: a systematic review. Br. J. Ophthalmol. *91*, 1177–1182.
13. Bates, P.J., Laber, D.A., Miller, D.M., Thomas, S.D., and Trent, J.O. (2009). Discovery and development of the G-rich oligonucleotide AS1411 as a novel treatment for cancer. Exp. Mol. Pathol. *86*, 151–164.
14. Cheng, Y., Zhao, G., Zhang, S., Nigim, F., Zhou, G., Yu, Z., Song, Y., Chen, Y., and Li, Y. (2016). AS1411-Induced Growth Inhibition of Glioma Cells by Up-Regulation of p53 and Down-Regulation of Bcl-2 and Akt1 via Nucleolin. PLoS One *11*, e0167094.
15. Rosenberg, J.E., Bambury, R.M., Van Allen, E.M., Drabkin, H.A., Lara, P.N., Harzstark, A.L., Wagle, N., Figlin, R.A., Smith, G.W., Garraway, L.A., et al. (2014). A phase II trial of AS1411 (a novel nucleolin-targeted DNA aptamer) in metastatic renal cell carcinoma. Invest. N. Drugs *32*, 178–187.
16. Röthlisberger, P., and Hollenstein, M. (2018). Aptamer chemistry. Adv. Drug Deliv. Rev. *134*, 3–21.
17. Harp, J.M., Guenther, D.C., Bisbe, A., Perkins, L., Matsuda, S., Bommineni, G.R., Zlatev, I., Foster, D.J., Taneja, N., Charisse, K., et al. (2018). Structural basis for the synergy of 4'- and 2'-modifications on siRNA nuclease resistance, thermal stability and RNAi activity. Nucleic Acids Res. *46*, 8090–8104.
18. Koller, E., Vincent, T.M., Chappell, A., De, S., Manoharan, M., and Bennett, C.F. (2011). Mechanisms of single-stranded phosphorothioate modified antisense oligonucleotide accumulation in hepatocytes. Nucleic Acids Res. *39*, 4795–4807.
19. Jepsen, J.S., Sørensen, M.D., and Wengel, J. (2004). Locked nucleic acid: a potent nucleic acid analog in therapeutics and biotechnology. Oligonucleotides *14*, 130–146.
20. Keefe, A.D., Pai, S., and Ellington, A. (2010). Aptamers as therapeutics. Nat. Rev. Drug Discov. *9*, 537–550.
21. Da Pieve, C., Blackshaw, E., Missailidis, S., and Perkins, A.C. (2012). PEGylation and biodistribution of an anti-MUC1 aptamer in MCF-7 tumor-bearing mice. Bioconjug. Chem. *23*, 1377–1381.
22. Haruta, K., Otaki, N., Nagamine, M., Kayo, T., Sasaki, A., Hiramoto, S., Takahashi, M., Hota, K., Sato, H., and Yamazaki, H. (2017). A Novel PEGylation Method for Improving the Pharmacokinetic Properties of Anti-Interleukin-17A RNA Aptamers. Nucleic Acid Therapeut. *27*, 36–44.
23. Takafuji, Y., Jo, J.-I., and Tabata, Y. (2011). Simple PEG modification of DNA aptamer based on copper ion coordination for tumor targeting. J. Biomater. Sci. Polym. Ed. *22*, 1179–1195.
24. Wang, Y., Wang, D., Lin, J., Lyu, Z., Chen, P., Sun, T., Xue, C., Mojtabavi, M., Vedadghavami, A., Zhang, Z., et al. (2022). A Long-Circulating Vector for Aptamers Based upon Polyphosphodiester-Backboned Molecular Brushes. Angew Chem. Int. Ed. Engl. *61*, e202204576.
25. Povsic, T.J., Vavalle, J.P., Aberle, L.H., Kasprzak, J.D., Cohen, M.G., Mehran, R., Bode, C., Buller, C.E., Montalescot, G., Cornel, J.H., et al. (2013). A Phase 2, randomized, partially blinded, active-controlled study assessing the efficacy and safety of variable anticoagulation reversal using the REG1 system in patients with acute coronary syndromes: results of the RADAR trial. Eur. Heart J. *34*, 2481–2489.
26. Ding, D., Yang, C., Lv, C., Li, J., and Tan, W. (2020). Improving Tumor Accumulation of Aptamers by Prolonged Blood Circulation. Anal. Chem. *92*, 4108–4114.
27. Jin, C., Zhang, H., Zou, J., Liu, Y., Zhang, L., Li, F., Wang, R., Xuan, W., Ye, M., and Tan, W. (2018). Floxuridine Homomeric Oligonucleotides "Hitchhike" with Albumin In Situ for Cancer Chemotherapy. Angew Chem. Int. Ed. Engl. *57*, 8994–8997.
28. Yang, C., Zhao, H., Sun, Y., Wang, C., Geng, X., Wang, R., Tang, L., Han, D., Liu, J., and Tan, W. (2022). Programmable manipulation of oligonucleotide-albumin interaction for elongated circulation time. Nucleic Acids Res. *50*, 3083–3095.
29. Malam, Y., Loizidou, M., and Seifalian, A.M. (2009). Liposomes and nanoparticles: nanosized vehicles for drug delivery in cancer. Trends Pharmacol. Sci. *30*, 592–599.
30. Absar, S., Nahar, K., Choi, S., Ahsan, F., Yang, V.C., and Kwon, Y.M. (2014). Serum albumin-protamine conjugate for biocompatible platform for targeted delivery of therapeutic macromolecules. J. Biomed. Mater. Res. *102*, 2481–2490.
31. Caspersen, M.B., Kuhlmann, M., Nicholls, K., Saxton, M.J., Andersen, B., Bunting, K., Cameron, J., and Howard, K.A. (2017). Albumin-based drug delivery using cysteine 34 chemical conjugates - important considerations and requirements. Ther. Deliv. *8*, 511–519.
32. Wall, A., Nicholls, K., Caspersen, M.B., Skrivergaard, S., Howard, K.A., Karu, K., Chudasama, V., and Baker, J.R. (2019). Optimised approach to albumin-drug conjugates using monobromomaleimide-C-2 linkers. Org. Biomol. Chem. *17*, 7870–7873.
33. Kuhlmann, M., Hamming, J.B.R., Voldum, A., Tsakiridou, G., Larsen, M.T., Schmøkel, J.S., Sohn, E., Bienk, K., Schaffert, D., Sørensen, E.S., et al. (2017). An Albumin-Oligonucleotide Assembly for Potential Combinatorial Drug Delivery and Half-Life Extension Applications. Mol. Ther. Nucleic Acids *9*, 284–293.
34. Wienkers, L.C., and Heath, T.G. (2005). Predicting in vivo drug interactions from in vitro drug discovery data. Nat. Rev. Drug Discov. *4*, 825–833.
35. Zheng, Y.F., Bae, S.H., Huang, Z., Chae, S.U., Jo, S.J., Shim, H.J., Lee, C.B., Kim, D., Yoo, H., and Bae, S.K. (2020). Lack of Correlation between In Vitro and In Vivo Studies on the Inhibitory Effects of (−)-Sophoranone on CYP2C9 is Attributable to Low Oral Absorption and Extensive Plasma Protein Binding of (−)-Sophoranone. Pharmaceutics *12*, 328.
36. Bowman, C.M., and Benet, L.Z. (2019). In Vitro-In Vivo Inaccuracy: The CYP3A4 Anomaly. Drug Metab. Dispos. *47*, 1368–1371.
37. Obrezanova, O., Martinsson, A., Whitehead, T., Mahmoud, S., Bender, A., Miljković, F., Grabowski, P., Irwin, B., Oprisiu, I., Conduit, G., et al. (2022). Prediction of In Vivo

Pharmacokinetic Parameters and Time-Exposure Curves in Rats Using Machine Learning from the Chemical Structure. Mol. Pharm. *19*, 1488–1504.

38. Saeidnia, S., Manayi, A., and Abdollahi, M. (2015). From in vitro Experiments to in vivo and Clinical Studies; Pros and Cons. Curr. Drug Discov. Technol. *12*, 218–224.
39. Pardridge, W.M., Triguero, D., Yang, J., and Cancilla, P.A. (1990). Comparison of in vitro and in vivo models of drug transcytosis through the blood-brain barrier. J. Pharmacol. Exp. Therapeut. *253*, 884–891.
40. Gomes, C.M., Abrunhosa, A.J., Ramos, P., and Pauwels, E.K.J. (2011). Molecular imaging with SPECT as a tool for drug development. Adv. Drug Deliv. Rev. *63*, 547–554.
41. Pérez-Medina, C., Teunissen, A.J.P., Kluza, E., Mulder, W.J.M., and van der Meel, R. (2020). Nuclear imaging approaches facilitating nanomedicine translation. Adv. Drug Deliv. Rev. *154–155*, 123–141.
42. Xia, W., Singh, N., Goel, S., and Shi, S. (2023). Molecular imaging of innate immunity and immunotherapy. Adv. Drug Deliv. Rev. *198*, 114865.
43. Figueiredo, J., Lopes-Nunes, J., Carvalho, J., Antunes, F., Ribeiro, M., Campello, M.P.C., Paulo, A., Paiva, A., Salgado, G.F., Queiroz, J.A., et al. (2019). AS1411 derivatives as carriers of G-quadruplex ligands for cervical cancer cells. Int. J. Pharm. *568*, 118511.
44. Khademi, Z., Lavaee, P., Ramezani, M., Alibolandi, M., Abnous, K., and Taghdisi, S.M. (2020). Co-delivery of doxorubicin and aptamer against Forkhead box M1 using chitosan-gold nanoparticles coated with nucleolin aptamer for synergistic treatment of cancer cells. Carbohydr. Polym. *248*, 116735.
45. Waaijer, S.J.H., Kok, I.C., Eisses, B., Schröder, C.P., Jalving, M., Brouwers, A.H., Lub-de Hooge, M.N., and de Vries, E.G.E. (2018). Molecular Imaging in Cancer Drug Development. J. Nucl. Med. *59*, 726–732.
46. Willmann, J.K., van Bruggen, N., Dinkelborg, L.M., and Gambhir, S.S. (2008). Molecular imaging in drug development. Nat. Rev. Drug Discov. *7*, 591–607.
47. Sarmento-Ribeiro, A.B., Scorilas, A., Gonçalves, A.C., Efferth, T., and Trougakos, I.P. (2019). The emergence of drug resistance to targeted cancer therapies: Clinical evidence. Drug Resist. Updates *47*, 100646.
48. Min, H.-Y., and Lee, H.-Y. (2022). Molecular targeted therapy for anticancer treatment. Exp. Mol. Med. *54*, 1670–1694.
49. Andersen, J.T., Dalhus, B., Cameron, J., Daba, M.B., Plumridge, A., Evans, L., Brennan, S.O., Gunnarsen, K.S., Bjørås, M., Sleep, D., and Sandlie, I. (2012). Structure-based mutagenesis reveals the albumin-binding site of the neonatal Fc receptor. Nat. Commun. *3*, 610.
50. Ni, S., Zhuo, Z., Pan, Y., Yu, Y., Li, F., Liu, J., Wang, L., Wu, X., Li, D., Wan, Y., et al. (2021). Recent Progress in Aptamer Discoveries and Modifications for Therapeutic Applications. ACS Appl. Mater. Interfaces *13*, 9500–9519.
51. Ding, Y., Han, Y., Wang, R., Wang, Y., Chi, C., Zhao, Z., Zhang, H., Wang, W., Yin, L., and Zhou, J. (2017). Rerouting Native HDL to Predetermined Receptors for Improved Tumor-Targeted Gene Silencing Therapy. ACS Appl. Mater. Interfaces *9*, 30488–30501.
52. An, S., Zhang, D., Zhang, Y., Wang, C., Shi, L., Wei, W., Huang, G., and Liu, J. (2022). GPC3-targeted immunoPET imaging of hepatocellular carcinomas. Eur. J. Nucl. Med. Mol. Imag. *49*, 2682–2692.
53. Hu, B., Liu, T., Li, L., Shi, L., Yao, M., Li, C., Ma, X., Zhu, H., Jia, B., and Wang, F. (2022). IgG-Binding Nanobody Capable of Prolonging Nanobody-Based Radiotracer Plasma Half-Life and Enhancing the Efficacy of Tumor-Targeted Radionuclide Therapy. Bioconjug. Chem. *33*, 1328–1339.
54. Hu, G., Zhu, W., Liu, Y., Wang, Y., Zhang, Z., Zhu, S., Duan, W., Zhou, P., Fu, C., Li, F., and Huo, L. (2022). Development and comparison of three 89Zr-labeled anti-CLDN18.2 antibodies to noninvasively evaluate CLDN18.2 expression in gastric cancer: a preclinical study. Eur. J. Nucl. Med. Mol. Imag. *49*, 2634–2644.
55. Kwak, G., Kim, H., Park, J., Kim, E.H., Jang, H., Han, G., Wang, S.Y., Yang, Y., Chan Kwon, I., and Kim, S.H. (2021). A Trojan-Horse Strategy by In Situ Piggybacking onto Endogenous Albumin for Tumor-Specific Neutralization of Oncogenic MicroRNA. ACS Nano *15*, 11369–11384.
56. Tan, H., Su, W., Zhang, W., Zhang, J., Sattler, M., and Zou, P. (2021). Albumin-binding domain extends half-life of glucagon-like peptide-1. Eur. J. Pharmacol. *890*, 173650.
57. Bai, J.-W., Qiu, S.-Q., and Zhang, G.-J. (2023). Molecular and functional imaging in cancer-targeted therapy: current applications and future directions. Signal Transduct. Targeted Ther. *8*, 89.
58. Maor, Y., and Malnick, S. (2013). Liver injury induced by anticancer chemotherapy and radiation therapy. Int. J. Hepatol. *2013*, 815105.
59. Mangeat, T., Gracia, M., Pichard, A., Poty, S., Martineau, P., Robert, B., and Deshayes, E. (2023). Fc-engineered monoclonal antibodies to reduce off-target liver uptake. EJNMMI Res. *13*, 81.
60. Miyauchi, S., Kim, S.-J., Lee, W., and Sugiyama, Y. (2022). Consideration of albumin-mediated hepatic uptake for highly protein-bound anionic drugs: Bridging the gap of hepatic uptake clearance between in vitro and in vivo. Pharmacol. Ther. *229*, 107938.